

Article

Investigation for Sidewall Roughness Caused Optical Scattering Loss of Silicon-on-Insulator Waveguides with Confocal Laser Scanning Microscopy

Hongpeng Shang, Degui Sun *, Peng Yu, Bin Wang, Ting Yu, Tiancheng Li and Huilin Jiang

Schools of Optoelectronic Engineering, Science and Mechatronic Engineering, Changchun University of Science and Technology, Changchun 130022, China; shanghongpeng@126.com (H.S.); 13620788904@163.com (P.Y.); dawangbin123@163.com (B.W.); yutingguangxue@163.com (T.Y.); 15568553366@163.com (T.L.); HLJIANG@cust.edu.cn (H.J.)

* Correspondence: sundg@cust.edu.cn

Received: 4 February 2020; Accepted: 29 February 2020; Published: 4 March 2020



Abstract: Sidewall roughness-caused optical loss of waveguides is one of the critical limitations to the proliferation of the silicon photonic integrated circuits in fiber-optic communications and optical interconnects in computers, so it is imperative to investigate the distribution characteristics of sidewall roughness and its impact upon the optical losses. In this article, we investigated the distribution properties of waveguide sidewall roughness (SWR) with the analysis for the three-dimensional (3-D) SWR of dielectric waveguides, and, then the accurate SWR measurements for silicon-on-insulator (SOI) waveguide were carried out with confocal laser scanning microscopy (CLSM). Further, we composed a theoretical/experimental combinative model of the SWR-caused optical propagation loss. Consequently, with the systematic simulations for the characteristics of optical propagation loss of SOI waveguides, the two critical points were found: (i) the sidewall roughness-caused optical loss was synchronously dependent on the correlation length and the waveguide width in addition to the SWR and (ii) the theoretical upper limit of the correlation length was the bottleneck to compressing the roughness-induced optical loss. The simulation results for the optical loss characteristics, including the differences between the TE and TM modes, were in accord with the experimental data published in the literature. The above research outcomes are very sustainable to the selection of coatings before/after the SOI waveguide fabrication.

Keywords: sidewall roughness; optical scattering loss; silicon-on-insulator waveguide

1. Introduction

Higher and higher integration density is the long-standing goal of the optical integrated circuits in the modern optical communications systems [1,2]. Since the beginning of the 21st century, the silicon-on-insulator (SOI) waveguide-based photonic integrated circuits (PIC) have shown unprecedented potential. Therefore, as the main source of optical propagation loss (OPL) of waveguides, the surface roughness-caused optical scattering loss has been attracting much research, and several theoretical models for defining the relations between the optical propagation losses and the sidewall roughness (SWR) of a waveguide are proposed. Illustratively, the average optical loss of SOI strip waveguides is around 0.24 dB/mm [3–5], while that of the small area square SOI waveguides is around 1.3 dB/mm [6]. Thus, it is of paramount importance to be able to quantitatively predict the optical loss on the magnitude and distribution property of waveguide SWR so that we can realize the expected performance specifications of PIC devices.

In the study of the mechanisms of the optical propagation loss caused by waveguide SWR, Marcuse proposed the earliest theory in 1969 in which the optical power ratio at the nonuniform

boundary was considered [7]. In 1994, Payne and Lacey proposed a theoretical model for defining the relation between the optical scattering loss and sidewall roughness of a waveguide based on a combination of the spectral density of the nonuniform edge of the waveguide, and the autocorrelation of roughness caused wave scattering, so it was then commonly accepted and referred to as the Payne-Lacey (PL) model [8]. However, both the Marcuse model and PL model have a similar shortcoming that the light wave at the waveguide boundary is not specified, and the waveguide channel is simplified to be a two-dimensional (2-D) structure, where the SWR is assumed to have a uniform distribution. Since the beginning of the 21st century, there has been a strong attempt to extend the PL model into the three-dimensional (3-D) structures and consider the other elements causing the optical loss of waveguide in addition to the SWR [9–12]. In 2005, Barwicz and Haus carried out their theoretical work based on the 3-D interaction between the polarized Poynting vector and the vertical shape of the field (VSF) so that they could give rise to the more detailed simulations of the OPL values of both the low and high index-contrast waveguides [9]. In 2006, Poulton et al. gave a more powerful explanation as that the OPL caused by the SWR was from the two conversions: the conversion from a guided-mode to a radiation mode and the conversion from the radiation mode to a leaky mode, so that they could accurately compute the electric fields with the finite-difference time-domain (FDTD) method [10]. Especially, for the SOI waveguides, in 2008, Schmid et al. employed the non-uniform waveguide boundaries to study the scattering loss [11], and, in 2009, Yap et al. first led the optical scattering loss of SOI waveguides to the synchronous dependences the SWR and the channel width [12]. Until 2019, we first published the measurement metrology of the waveguide SWR with a confocal laser scanning microscopy (CLSM) technique [13].

In this article, we theoretically investigated the SWR property of dielectric waveguides by analyzing its components in the horizontal and vertical direction. Then, we measured the 3-D distribution of waveguide SWR with the CLSM technique and constructed a theoretical/experimental ensemble model for defining the SWR-caused optical propagation loss. This model was an extended version of the PL model with the 3-D distribution of SWR. As a result, with such a combinative model, we simulated the dependences of the optical propagation loss coefficient of the waveguide on the SWR distribution and the width. Finally, we analyzed the theoretical and experimental results.

2. Theoretical Analysis for Waveguide Sidewall Roughness

2.1. Analysis for the PL Model

An equivalent rectangular 3-D vision of an SOI waveguide is shown in Figure 1a, where n_1 and n_2 are the refractive indices of the core and cladding layers, respectively, and $2d$ is the width of the waveguide. The SWR of a waveguide was caused by the inductively coupled plasma (ICP)-etching, as shown in Figure 1b, then as shown in Figure 1c, the distributions of the SWR at the vertical and horizontal directions were probably different from each other.

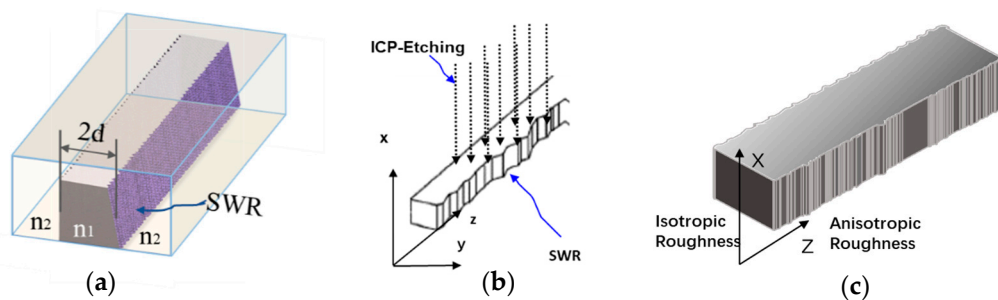


Figure 1. Sidewall roughness (SWR) of silicon-on-insulator (SOI) waveguide: (a) the schematic three-dimensional (3-D) equivalent rectangular waveguide with SWR; (b) the ICP-etching to a waveguide sidewall; (c) the distributions of the SWR at x - and z -coordinate.

In accordance with the 3-D simulations of radiation mode, the three linear polarization states (x , y , and z) could cause the different profiles of the radiation mode [8,9]. The exponential form of the PL model was used to define a space distribution Equation (1) for an interest. The power spectral density of the roughness was of interest in the optical scattering loss, then the Fourier transform of the autocorrelation function of the roughness was expressed to be Equation (2) [8,9]:

$$R(u) \approx \sigma^2 \exp(-|u|/L_c) \quad (1)$$

$$R(\xi) \approx 2\sigma^2 L_c / (1 + L_c^2 \xi^2) \quad (2)$$

where σ is the root-mean-square (rms) roughness, L_c is the correlation length of the roughness with the assumption that there is no correlation between the two sidewalls, u is the space variable of a waveguide sidewall, and ξ is the space-frequency of the power spectral function of roughness. If the wavelength of the light wave in air was λ , with the wavenumber as $k_0 = 2\pi/\lambda$ and the finite difference processing of beam propagation method (FD-BPM), we obtained the effective index N_{eff} of a single guided-mode, and further with the propagation constant of this guided-mode $\beta = k_0 \cdot N_{eff}$, we cited three dimensionless parameters h , V , and p of guided-mode defined by the PL model as [9]

$$h = d \sqrt{n_1^2 k_0^2 - \beta^2}, \quad V = k_0 d \sqrt{n_1^2 - n_2^2} \quad \text{and} \quad p = d \sqrt{\beta^2 - n_2^2 k_0^2} \quad (3)$$

where h and p are the very popular parameters, defining the guided mode field in the literature on optical waveguides [1,2]. V is the product of three elements: the numerical aperture $\sqrt{n_1^2 - n_2^2}$ of a symmetric planar waveguide, d is the radius (or half a width) of the waveguide core, and k_0 is the wave number in the air. Further, we obtained the dimensionless parameters as:

$$\Delta = (n_1^2 - n_2^2) / (2n_1^2), \quad x = p(L_c/d), \quad \gamma = (n_2 V) / (n_1 p \sqrt{\Delta}) \quad (4)$$

Consequently, for the two-SWR-induced optical scattering loss, with the above definitions for the guided-mode profile defined by Equations (3) and (4) and a combination of the PL model (1)–(4), the Yap improvement for the optical loss coefficient dependence on the SWR was expressed as [12]

$$\alpha_{PL}(TE/TM) = \frac{4.34\sigma_{2D}^2}{\sqrt{2}d^4\beta_{TE/TM}} g(V) \cdot f_e(x, \gamma) \quad (5)$$

where σ_{2D} is the SWR defined in the 2-D form, the loss coefficient is in dB/cm, and the functions $g(V)$ and $f_e(x, \gamma)$ are defined by

$$g(V) = \frac{h^2 V^2}{1 + p^2} \quad \text{and} \quad f_e(x, \gamma) = \frac{\{[(1 + x^2)^2 + 2x^2\gamma^2]^{1/2} + 1 - x^2\}^{1/2}}{[(1 + x^2)^2 + 2x^2\gamma^2]^{1/2}} \quad (6)$$

The model defined by Equations (5) and (6) might be referred to as a Yap-form PL model.

2.2. Three-Dimensional Model for the SWR-caused Optical Scattering Loss

In the roughness-improved PL model, the correlation length of sidewall roughness L_c is a paramount important parameter [9]. Before 2000, for a low index-contrast waveguide, such as silica-waveguide, L_c was observed to be a few micrometers, and even the values less than 500 nm were ever exploited, and meanwhile, the optical scattering loss was determined to be a forward-scattering process, where $L_c \approx 1/2\beta$ that matched with the maximum attenuation [14]. In contrast, Barwicz and Haus studied the 3-D optical scattering process for both the high and low index-contrast waveguides with respect to three L_c values as 1, 50, and 150 nm [9]. In the Barwicz-Haus's 3-D theory, the optical scattering loss is thought to be caused by a radiative mode coupled from a guided mode, meanwhile,

for straight roughed waveguides, the phase-matching condition between the guided and the radiated modes allows only a narrow range of spectral frequencies of roughness to produce radiation loss, then the estimated correlation length L_c value is in a range of $1/(\beta + n_2k_0) < L_c < 1/(\beta - n_2k_0)$. Consequently, for both the TE-like and TM-like modes, the SWR-induced optical scattering loss was related to both the y - and z -components of roughness, so the dependences of the optical intensity loss coefficients $\alpha_{3D}(TE/TM)$ on the SWR $\sigma_{3D}(TE/TM)$ could be expressed as

$$\alpha_{3D}(TE/TM) = 4.34 \left(\frac{\sigma_{3D}^2(TE/TM)}{\sqrt{2}d^4\beta_{TE/TM}} g(V) \cdot f_e(x, \gamma) \right) \quad (7)$$

Hence, the new model Equation (7) was the combination of the Yap-form PL model and the 3-D SWR distribution. In this model, the optical loss coefficient was in dB/cm.

3. Measurements for the Roughness Characteristics with CLSM

3.1. Experimental Measurement

Figure 2 shows the surface roughness measurement mechanism with a CLSM system: (a) is a schematic optical imaging system in which the laser beam as a probe has a wavelength of 405 nm, and the section of scanning is set 10 nm, and the spot size of the focused laser beam is defined by the full width at the half-maximum (FWHM) of the laser intensity distribution, (b) is an illustrative sample of the retrieved image in the CLSM measurement, and (c) is the standard definition of the peak-to-valley (P-V) roughness.

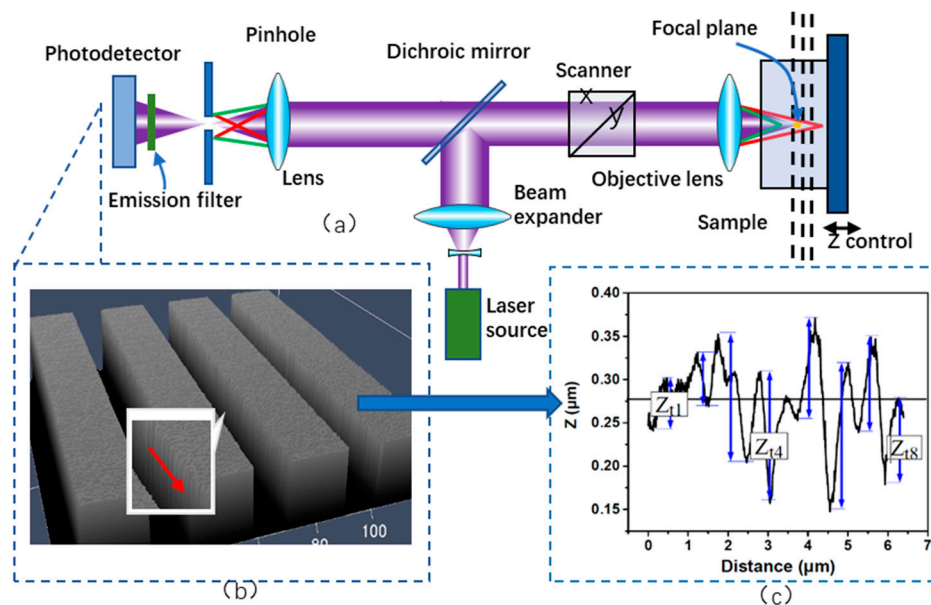


Figure 2. CLSM (confocal laser scanning microscopy) measurement and the definition for surface roughness: (a) The schematic optical imaging system, (b) the retrieved image of CLSM-measured result of an object, and (c) the definition for the fabricated surface roughness.

In the CLSM metrology, the roughness is defined as a root mean square (rms) PS_z of all the P-V periods as [13,15]

$$PS_z = (1/N) \sqrt{\left(\sum_{i=1}^N R_{ai}^2 \right)} \quad (8)$$

where R_{ai} is the average roughness at the i^{th} scanned period in the CLSM measurement. In this definition of roughness, the PS_z could be taken as a one-dimensional (1-D) roughness σ_{1D} , then the 2-D average roughness σ_{2D} and the 3-D average roughness σ_{3D} are defined as

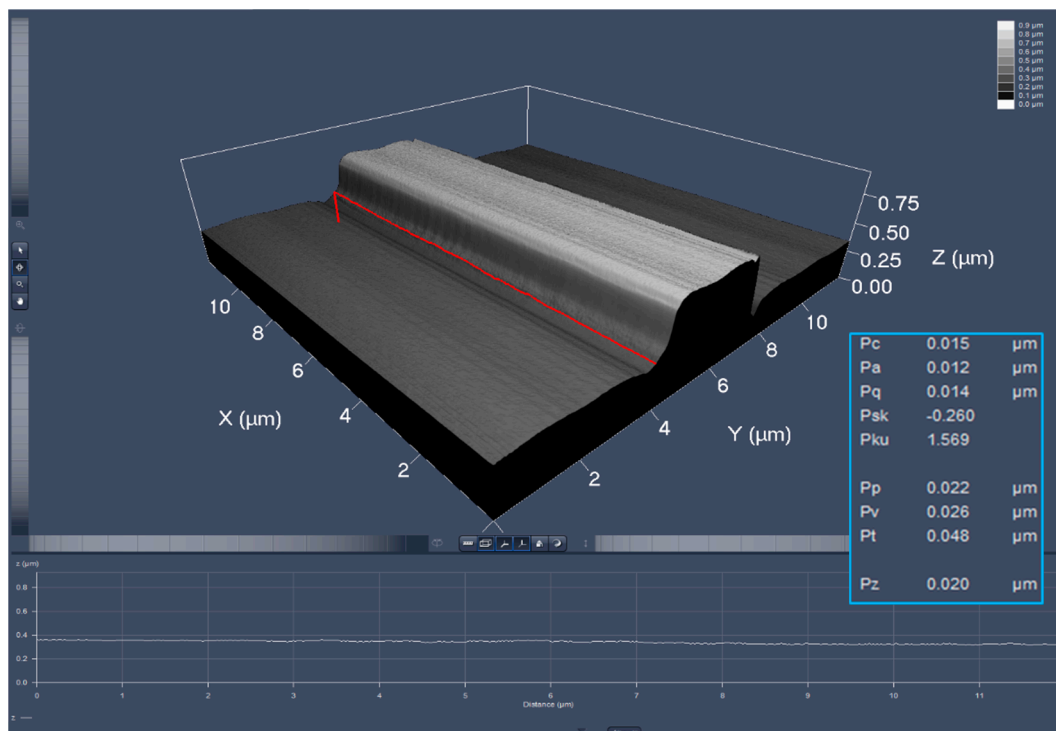
$$\sigma_{2D} = (1/m) \sum_{j=1}^m PS_z(a_j) \quad (9a)$$

$$\sigma_{3D} = (1/n) \sum_{k=1}^n \sigma_{2D}(ak) \quad (9b)$$

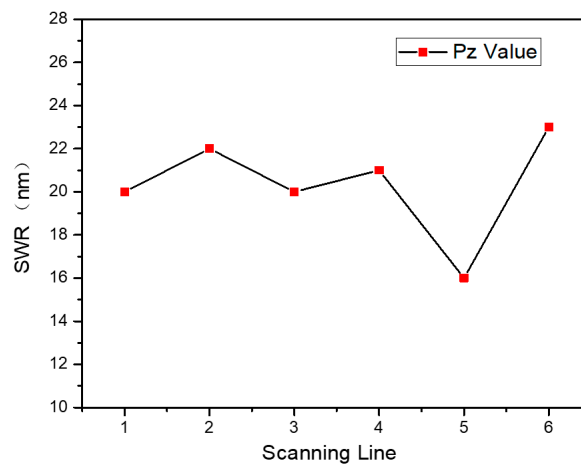
3.2. Experimental Measurements for the SWR of SOI Waveguide Sample

In this work, we selected the commercial CLSM tool—LSM710 that was produced by the ZEISS company. Then, the device sample for the CLSM measurements was selected by selecting an SOI-waveguide sample having a BOX layer of 2.0 and 1.5 μm , where the waveguide ribs having a width of 4.0 μm and a height of 0.5 μm were etched with the advanced ion etching—the inductively coupled plasma (ICP) etching technique. The CLSM measurements only showed the existing isotropic roughness, then we obtained the reconstructed image of the waveguide SWR, as shown in Figure 3a, and by scanning the measured area along a vertical direction at the $x = 100 \text{ nm}$ position, a line-scanning roughness was obtained as $P_z = 20 \text{ nm}$ from the data display. Then, in the same manner, we measured the other five lines with every 100 nm position change along the vertical direction for two reconstructed images (the total height of the etched SOI rib was 500 nm), and then the total 6 measured values are depicted in Figure 3b, which were in the range of 16–23 nm roughness and gave rise to an average isotropic SWR of 20.33 nm. First, we needed to clarify that the x coordinate in Figure 3 was the traveling direction z of the optical beam, the z and y coordinates of Figure 3 were the coordinates x and z of Figure 1, respectively. Then, we also noticed that the SWR values of the SOI waveguides were only in the range of a few tens of nanometers, which were much smaller than the CLSM-measured values of the silica waveguide etched by the traditional reactive ion etching (RIE) technique owing to the advanced etching technique ICP and the etched material of silicon [16,17]. Accordingly, the disparities of SWR distributions between the x and y coordinates existed.

Here, what needed to be clarified was that the measurement accuracy was 10 nm in the above measurements, but for the roughness smaller than 10 nm, the accuracy needed to be improved, which would be realized with the improvement of the laser FWHM values in both the lateral and axial directions. In addition, as shown in Figure 2a, in one CLSM measurement, we scanned the device sample having four equal size waveguides to acquire the data, but as shown in Figure 3a, only one waveguide was selected from the reconstructed CLSM image to analyze and measure the roughness. In order to analyze the SWR uniformity of one channel, several sections could be selected along the waveguide to obtain the average SWR value of each section, and then all the roughness results of all the sections could be compared. In the same manner, in order to analyze the SWR uniformity among all the four measured waveguides, the CLSM measured results of SWR for all the four waveguides could be carried out, and then all the roughness results could be compared.



(a)



(b)

Figure 3. CLSM Measurements and data process of SOI waveguide SWR: (a) is the reconstructed image of CLSM measurement, (b) is the isotropic roughness distribution of five measured spots.

4. Verifications for the SWR-caused Optical Propagation Loss

4.1. Simulations for the SWR-Caused Optical Scattering Loss

In the CLSM system shown in Figure 2, the measurements shown in Figure 3 presented that an SOI waveguide generally had much lower SWR value than silicon dioxide (SiO₂) waveguides, even when they were fabricated under the same etching technique, ICP. Thus, it could be forecasted that the waveguide dimensions of both core and cladding layers of a waveguide system probably have significant effects on the optical scattering loss apart from the sidewall roughness itself.

Based on the optical performance of the real SOI waveguide functional device, we selected an SOI waveguide sample having the rib width and height of 4.0 and 0.5 μm, respectively; at 1550 nm wavelength, the refractive index silicon film was 3.4777 [18], and the refractive index of both the

BOX layer and upper cladding layer was 1.4394 and 1.4449 for TE and TM modes, respectively; then, the effective indices of 3.3254 and 3.3168, respectively, were obtained with the simulation of beam propagation method (BPM) software. Further, by selecting the 2-D SWR construction defined by Equation (9a) and with the improved model Equation (7), we obtained the simulation results of the SWR dependences of the OPL coefficient, as shown in Figure 4a. Note from Figure 4a that the SWR-induced OPL of TM-mode was higher than that of TE mode for the SOI waveguide, which was not consistent with the results published in the literature [11,12]. Thus, it turned out that both the core and cladding layers of the waveguide system probably had significant effects on the optical scattering loss apart from the sidewall roughness itself. In contrast, by selecting the 3-D SWR construction defined by Equation (9b) and with the improved model Equation (7) of the SWR-caused OPL, we obtained the simulation results of the roughness dependences of the OPL coefficient for the same waveguide sample, as shown in Figure 4b. Note from Figure 4b that with the consideration of the 3-D construction of the roughness, there were two different points of the OPL coefficient between TE and TM modes. One was that the absolute TE-TM difference of the 3-D roughness was relatively larger than that of the 2-D roughness, and the other was that the OPL of TE mode was higher than that of TM mode, which was inverse to the 2-D roughness, but it was really in accord with the measured values published in the literature [11,12]. However, for the measured SWR value in Figure 3, ~20 nm, the OPL values for both the 2-D and 3-D SWR constructions were in the range of 3–3.5 dB/cm.

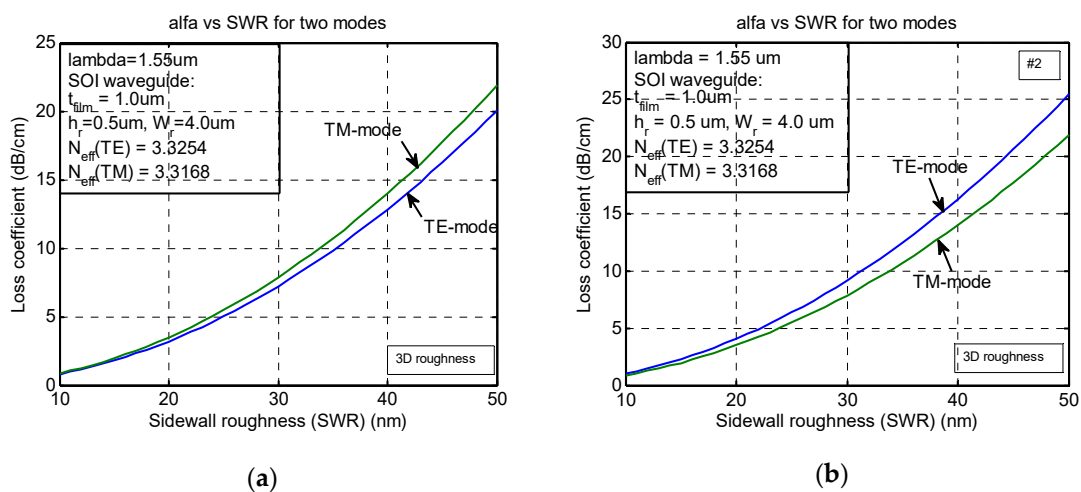


Figure 4. Simulations for the optical loss coefficient of SOI waveguide vs. SWR for two SWR constructions: (a) the 2D SWR, (b) the 3D-SWR.

As mentioned above, the measurements showed that the SOI-waveguides sample fabricated in the ICP technique only had an average roughness of 20 nm, namely, the 2-D statistic values at both the horizontal and vertical directions were the same. Then, with the 3-D roughness construction and the same values of the SOI waveguide parameters as used for the simulations in Figure 4b, we simulated the synchronous dependences of the roughness-induced optical propagation loss coefficient on both the correlation length L_c and the rib width $W_r(2d)$ of the waveguide, as shown in Figure 5.

The most impressive finding from Figure 5 was that once the SWR values were given, the correlation length L_c had the most dominant impact, and the waveguide width $2d$ had the nonignorable impact upon the roughness-induced OPL in addition to the SWR itself. Accordingly, based on the optimal states of both the SWR and geometrical configuration of a waveguide, to significantly increase the correlation length L_c of the waveguide was the most effective metrology to completely solving the OPL of SOI waveguides. However, the L_c is a function pertaining to the SWR and the dimension of the waveguide [8].

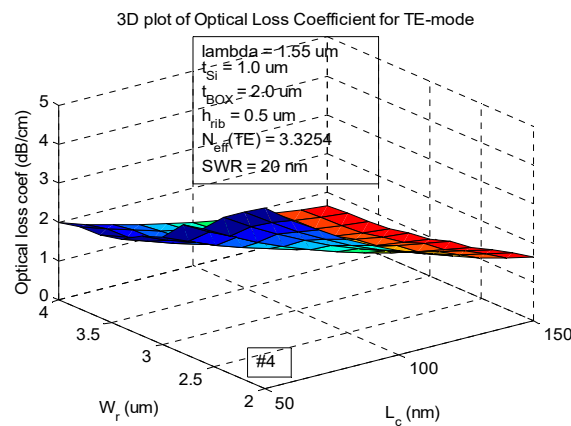


Figure 5. Simulations for the dependences of optical loss of SOI waveguide on both the correlation length and the waveguide width apart from SWR itself of the TE-mode of the waveguide.

4.2. Experimental Measurements for the Optical Propagation Loss of an SOI Waveguide

Among the methods for measuring the OPL of waveguides, the Fabry–Perot (F-P) resonance method is the most appropriate approach when the SOI waveguide chip has a length of around 1 cm due to the ultrahigh fiber-waveguide but coupling loss [18]. With this method, the two ends of the waveguide were polished to form an optical F-P cavity for an optical signal launched into the waveguide. When the optical length of the cavity was continuously changed with either the refractive index of the waveguide material or the wavelength of the optical signal, the optical intensity transmission coefficient of resonance output of the cavity would present a form of the periodic wave. In this method, if the wavelength λ , the waveguide length l_{WG} , and the intensity reflection coefficient R_{end} of two waveguide ends were given, the resonance output intensity of the waveguide cavity was defined by Feuchter and Thirstrup in 1994 [19]. Then, with the special transmittance values, T_{max} and T_{min} , its optical propagation loss α coefficient was obtained. In the experiments, we uniformly changed the refractive index of an SOI waveguide by heating the waveguide with a length of 8.5 mm, then the optical resonant output curve with the temperature was obtained, as shown in Figure 6, and consequently, the optical propagation loss of $\alpha = \sim 3.1$ dB/cm was reached. In the SWR measurement and prediction of the SWR-caused OPL, this result was very agreeable with the numerical simulation results, shown in Figures 4 and 5, in which the average 20.33 nm anisotropic SWR based on the CLSM measurements were exploited and the OPL distributions of 3.0–3.5 dB/cm that were obtained with the 3-D construction in Figure 4b. From the view of the fabrication of SOI waveguides, the OPL of 3.1 dB/cm was relatively lower than the value of 3.6 ± 0.1 dB/cm, published in 2002 [20], and relatively higher than the value of around 1.4 dB/cm, published in 2016 [21]. So, the ICP fabrication of the waveguide samples employed in this work still needs to be improved.

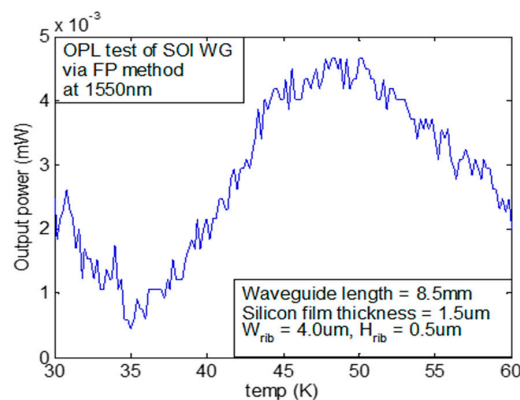


Figure 6. Measurement output curve of Fabry–Perot (F-P) resonance of the SOI waveguide vs. temperature.

5. Conclusions

In this work, the analyses for the ion etching-based SWR of a rectangular dielectric waveguide led to the categorization of the horizontal and vertical components, and the P-V definition of type surface roughness of CLSM measurements also showed the ability to scan the etched surface at the two directions. Then, the possible different contributions of two components to OPL of waveguide could be imaged and reconstructed as the measurement results. Therefore, with the accurate measured values of the SWR and the theoretical/experimental combinative model, the accurate OPL coefficient was composed, and the important simulation results of the SWR-caused optical loss were found with this model. Therefore, the conclusions obtained in this article are very sustainable in considering the ensemble effect of SWR and the SOI waveguide structure in the research and development of high-quality industrial devices and systems. As an additional conclusion from this work, the upper limit of the correlation length was calculated to be 130 nm, and in any similar work in the future, this parameter is necessary to be discussed. With the above simulation results and conclusions, the coating works of silicon dioxide films of both the BOX layer and the upper cladding layer could be specifically designed to compress the optical loss.

Author Contributions: Conceptualization, H.S. and D.S.; methodology, H.S., P.Y., B.W. and T.L.; validation, H.S. and D.S.; formal analysis, D.S., H.S. and H.J.; investigation, D.S., H.S. and T.Y.; data curation, H.S. and B.W.; writing—original draft preparation, H.S.; writing—review and editing, H.J. and D.S.; visualization, P.Y. All authors have read and agreed to the published version of the manuscript.

Funding: This work is co-sponsored by the Natural Science Foundation of Jilin Provincial Science & Technology (Foundation Grant: 20180101223JC).

Acknowledgments: The authors thank the Chang Guang Yuanchen Optoelectronics, Ltd., for their help in Si etching and PECVD coatings of SOI wafer samples. Else, the authors would like to thank Guozheng Wang of the School of Science at the CUST, China, for his help in wafer processing, and want to thank a graduate, Xueping Wang, for her support in testing.

Conflicts of Interest: The authors declare no conflict of interest.

References

1. Doerr, C.R.; Okamoto, K. Planar lightwave circuits in fiber-optic communications. In *Optical Fiber Telecommunications*; Kaminow, I., Li, T., Eds.; Academic Press/Elsevier: New York, NY, USA, 2008.
2. Murphy, E.J. *Optical Circuits and Components: Design and Applications*; Marcel Dekker, Inc.: New York, NY, USA, 1999.
3. Chrostowski, K.; Hochberg, M. Silicon photonics design: From devices to systems. In *Silicon Photonics: Fueling the Next Information Revolution*, 1st ed.; Innis, D., Rubenstein, R., Eds.; Cambridge University Press: Cambridge, UK, 2015; pp. 3–27.
4. Orcutt, J.S.; Moss, B.; Sun, C.; Leu, J.; Georgas, M.; Zraggen, J.S.E.; Li, H.; Sun, J.; Weaver, M.; Urošević, S.; et al. Open foundry platform for high-performance electronic-photonic integration. *Opt. Express* **2012**, *20*, 12222–12232. [[CrossRef](#)] [[PubMed](#)]
5. Dumon, P.; Bogaerts, W.; Wiaux, V.; Wouters, J.; Beckx, S.; Van Campenhout, J.; Taillaert, D.; Luyssaert, B.; Bienstman, P.; Van Thourhout, D.; et al. Low-loss SOI photonic wires and ring resonators fabricated with deep UV lithography. *IEEE Photonics Technol. Lett.* **2004**, *16*, 1328–1330. [[CrossRef](#)]
6. Tsuchizawa, T.; Yamada, K.; Fukuda, H.; Watanabe, T.; Takahashi, J.I.; Takahashi, M.; Shoji, T.; Tamechika, E.; Itabashi, S.I.; Morita, H. Microphotonics devices based on silicon microfabrication technology. *IEEE J. Sel. Top. Quantum Electron.* **2005**, *11*, 232–240. [[CrossRef](#)]
7. Marcuse, D. Radiation losses of dielectric waveguides in terms of the power spectrum of the wall distortion function. *Bell Syst. Technol. J.* **1969**, *48*, 3233–3244. [[CrossRef](#)]
8. Payne, F.P.; Lacey, J.P.R. A theoretical analysis of scattering loss from planar optical waveguides. *Opt. Quant. Electron.* **1994**, *26*, 977–986. [[CrossRef](#)]
9. Barwicz, T.; Haus, H.A. Three-dimensional analysis of scattering loss due to sidewall roughness in micro photonic waveguides. *IEEE J. Lightw. Technol.* **2005**, *3*, 2719–2732. [[CrossRef](#)]

10. Poulton, C.G.; Koos, C.; Fujii, M.; Pfrang, A.; Schimmel, T.; Leuthold, J.; Freude, W. Radiation models and roughness loss in high index-contrast waveguides. *IEEE J. Sel. Top. Quantum Electron.* **2006**, *12*, 1306–1321. [[CrossRef](#)]
11. Schmid, J.H.; Delège, A.; Lamontagne, B.; Lapointe, J.; Janz, S.; Cheben, P.; Densmore, A.; Waldron, P.; Xu, D.-X.; Yap, K.P. Interference effect in scattering loss of high-index-contrast planar waveguides caused by boundary reflections. *Opt. Lett.* **2008**, *33*, 1479–1481. [[CrossRef](#)] [[PubMed](#)]
12. Yap, K.P.; Delège, A.; Lapointe, J.; Lamontagne, B.; Schmid, J.H.; Waldron, P.; Syrett, B.A.; Janz, S. Correlation of scattering loss, sidewall roughness and waveguide width in silicon-on-insulator (SOI) ridge waveguides. *IEEE J. Lightw. Technol.* **2009**, *27*, 3999–4007.
13. Sun, D.G.; Shang, H.; Jiang, H.L. Effective metrology and standard of the surface roughness of micro/nanoscale waveguides with confocal laser scanning microscopy. *Opt. Lett.* **2019**, *44*, 747–750. [[CrossRef](#)] [[PubMed](#)]
14. Lee, K.K.; Lim, D.R.; Luan, H.-C.; Agarwal, A.; Foresi, J.; Kimerling, L.C. Effect of size and roughness on light transmission in a Si/SiO₂ waveguide: Experiments and model. *Appl. Phys. Lett.* **2000**, *39*, 2705–2718. [[CrossRef](#)]
15. Shang, H.; Sun, D.G.; Sun, Q.; Yu, P.; Gao, J.; Hall, T.J. Analysis for system errors in measuring sidewall angle of silica waveguides with confocal laser scanning microscope (CLSM). *Meas. Sci. Technol.* **2019**, *30*, 025004. [[CrossRef](#)]
16. Cardinaud, C.; Peignon, M.C.; Tessier, P.Y. Plasma etching: Principle, applications to micro- and nano-technologies. *Appl. Surf. Sci.* **2000**, *164*, 72–83. [[CrossRef](#)]
17. Brault, P.; Dumas, P.; Salvan, F. Roughness scaling of plasma-etched silicon surface. *J. Phys. Cond. Matter* **1998**, *10*, 27–38. [[CrossRef](#)]
18. Dwivedi, S.; Ruocco, A.; Vanslebrouck, M.; Spuesens, T.; Bienstman, P.; Dumon, P.; Van Vaerenbergh, T.; Bogaerts, W. Experimental extract of effective refractive index and thermo-optic coefficients of silicon-on-insulator waveguides using interferometer. *IEEE J. Lightwave Technol.* **2015**, *33*, 4471–4477. [[CrossRef](#)]
19. Feuchter, T.; Thirstrup, C. High precision planar waveguide propagation loss measurement technique using a Fabry-Perot cavity. *IEEE Photonics Technol. Lett.* **1994**, *6*, 1244–1247. [[CrossRef](#)]
20. Vlasov, V.A.; McNab, S.J. Losses in single-mode silicon-on-insulator strip waveguides and bends. *Opt. Express* **2002**, *12*, 1622–1631. [[CrossRef](#)] [[PubMed](#)]
21. Boeuf, F.; Cremer, S.; Temporiti, E.; Fere, M.; Shaw, M.; Baudot, C.; Vulliet, N.; Pinguet, T.; Mekis, A.; Masini, G.; et al. Silicon photonic R&D and manufacturing on 300-mm wafer platform. *IEEE J. Lightwave Technol.* **2016**, *33*, 286–295.

